Journal of Scientific Computing (2020) 83:1
https://doi.org/10.1007/s10915-020-01189-x

Galerkin Boundary Element Methods for High-Frequency Multiple-Scattering Problems

Fatih Ecevit[1] · **Akash Anand**[2] · **Yassine Boubendir**[3]

Received: 15 May 2019 / Revised: 23 February 2020 / Accepted: 11 March 2020 / Published online: 16 March 2020

Abstract
We consider high-frequency multiple-scattering problems in the exterior of two-dimensional smooth scatterers consisting of finitely many compact, disjoint, and strictly convex obstacles. To deal with this problem, we propose Galerkin boundary element methods, namely the *frequency-adapted Galerkin boundary element methods* and *Galerkin boundary element methods generated using frequency-dependent changes of variables*. For both of these new algorithms, in connection with each multiple-scattering iterate, we show that the number of degrees of freedom needs to increase as $\mathcal{O}(k^{\epsilon})$ (for any $\epsilon > 0$) with increasing wavenumber k to attain frequency-independent error tolerances. We support our theoretical developments by a variety of numerical implementations.

Keywords High-frequency · Multiple-scattering · Galerkin boundary element method

Mathematics Subject Classification 35P25 · 78M15 · 78M35

F. Ecevit's work was supported by The Scientific and Technological Research Council of Turkey through grant number TÜBİTAK-1001-117F056. A. Anand gratefully acknowledges support from IITK-ISRO Space Technology Cell through contract No. STC/MATH/2014100. Y. Boubendir's work was supported by the NSF through Grant DMS-1720014.

✉ Fatih Ecevit
fatih.ecevit@boun.edu.tr

Akash Anand
akasha@iitk.ac.in

Yassine Boubendir
boubendi@njit.edu

[1] Department of Mathematics, Boğaziçi University, Bebek TR, 34342 Istanbul, Turkey

[2] Department of Mathematics and Statistics, Indian Institute of Technology Kanpur, 327 Faculty Building, Kanpur, UP 208016, India

[3] Department of Mathematical Sciences, New Jersey Institute of Technology, University Heights, Newark, NJ 07102, USA

1 Introduction

Standard methods to deal with scattering problems are based on finite elements [7,19,34] and integral equations [3,6,10,13,41]. Finite elements require the construction of artificial interfaces along with absorbing boundary conditions in order to truncate the unbounded computational domain and account for the radiation condition at infinity [5,26,29–31]. In the case of multiple-scattering problems, the sizes of artificial interfaces increase due to the distance between obstacles. This results in a large bounded domain that will lead to a challenging computational linear system, especially at the high-frequency regime. For these reasons, integral equation formulations are better adapted to these kinds of problems. Moreover, in surface scattering problems considered herein, they provide a dimensional reduction in the computational domain since the solutions can be computed based on a knowledge of the densities confined to the surface of the scattering obstacles [18]. Nonetheless, they give rise to dense linear systems whose sizes increase as $\mathcal{O}(k^p)$ with increasing wavenumber k where p is the dimension of the computational manifold.

In the context of two-dimensional single-scattering problems relating to smooth convex obstacles, several high-frequency integral equation methods that incorporate the known asymptotic behavior of solutions and that thereby reduce the sizes of linear systems were designed in the last decades [1,2,12,21,23,24,28,38] (for similar approaches to scattering problems related with convex polygons or variations thereof, see [14–17,27,32,33,35–37,39] and the references therein). Among these algorithms, [1,2,12,21,38] are asymptotic since they approximate the solutions in the shadow regions, beyond the $\mathcal{O}(k^{-1/3})$ shadow boundaries, by zero. This, in turn, implies that the numerical solutions do not converge to the actual solutions for any fixed wavenumber k as the number of degrees of freedom goes to infinity. Moreover, the methods in [1,2,12,28,38] are not supported with rigorous convergence analyses. Indeed, while the developments in [11,12,28,38] have signaled the possibility of obtaining approximate solutions within prescribed error tolerances in frequency independent computational times, [21] has demonstrated that an upper bound on the number of degrees of freedom necessary to represent the unknown surface densities in these approaches is $\mathcal{O}(k^{1/9})$. Motivated by these observations, *frequency-adapted Galerkin boundary element methods* for the solution of single scattering problems were proposed and rigorously analyzed in [24]. These methods demand, for any smooth and strictly convex scatterer, an increase of $\mathcal{O}(k^\epsilon)$ (for any $\epsilon > 0$) in the number of degrees of freedom to maintain a prescribed accuracy independent of frequency. More recently, a class of *Galerkin boundary element methods based on frequency-dependent changes of variables* for the solution of single-scattering problems that display similar characteristics from both theoretical and practical perspectives were developed in [23]. The aim of this paper is to extend and rigorously analyze the single-scattering algorithms in [23,24] to encompass multiple-scattering problems.

The only numerical algorithm that has provided evidence on the spectral convergence of Neumann series for two convex obstacles, based on Nyström techniques, was designed in [9]. However, this approach is not supported by any type of analysis. On the other hand, in the context of a finite collection of two- or three-dimensional smooth compact and strictly convex obstacles, the problem of convergence of Neumann series was later addressed in [4,25] where the rigorous rate of convergence formulas on these orbits are derived.

In this paper, we extend the single-scattering algorithms in [23,24] to the case of multiple-scattering problems in the exterior of a finite collection of two-dimensional smooth compact and strictly convex obstacles. We use the theoretical results obtained in [25] in the numerical analysis of the Galerkin methods proposed to deal with multiple-scattering problems.

Specifically, here we prove for the numerical solution of each multiple-scattering iteration that the required number of degrees of freedom to represent each one of these iterates needs to increase only as $\mathcal{O}(k^{\epsilon})$ (for any $\epsilon > 0$) with increasing wavenumber k to obtain prescribed error tolerances independent of underlying frequency. Furthermore, following [22], we elucidate that incorporation of the leading terms in the asymptotic expansions of the multiple-scattering iterations [25] into the problem formulation reduces this bound to $\mathcal{O}(1)$ for e.g. the standard combined field integral equation [18]. While this is true of each multiple-scattering iterate, the direct use of Neumann series in configurations involving more than two obstacles is impractical as it requires the solution of an exponentially increasing number of single-scattering problems with an increasing number of reflections. In practical implementations, the algorithms proposed in this article must, therefore, be utilized in conjunction with the acceleration strategies recently developed in [8] (the approach there is based upon a Krylov subspace method implemented through a novel *identification process*—that retains the phase information associated with the multiple-scattering iterations and thereby preserves the frequency independent operation count—combined with a *dynamical* Kirchhoff preconditioning). In order to observe the true accuracy yielded by our algorithms, however, here we do not employ these acceleration strategies in our numerical implementations.

In summary, this paper fills an important gap in the literature by providing the first rigorous numerical algorithms capable of predicting multiple-scattering returns in essentially frequency independent computational times when combined with methods for the evaluation of highly oscillatory integrals (see e.g. [20] and the references therein).

The paper is organized as follows. In §2, we introduce the multiple-scattering problem along with appropriate integral equation formulations. In §3, we present the phase extraction for multiple-scattering iterations in the context of finitely many convex scatterers, and discuss wavenumber explicit derivative estimates of the related amplitudes [25]. In §4, we present the principles underlying the extensions of the *frequency-adapted Galerkin boundary element methods* [24] and *Galerkin boundary element methods based on frequency-dependent changes of variables* [23] to multiple-scattering problems and analyze their convergence characteristics. In §5, we present a variety of numerical examples confirming our theoretical results.

2 Multiple-Scattering Integral Equations

The two-dimensional exterior scattering problem considered herein is associated with a plane-wave incidence $u^{\text{inc}}(x,k) = e^{ik\alpha\cdot x}$ with direction α ($|\alpha| = 1$ and $k > 0$), impinging on a sound-soft, smooth, and compact scatterer K. In this case, the resulting *scattered field* u is sought to satisfy

$$\begin{cases} (\Delta + k^2)u(x,k) = 0, \quad x \in \mathbb{R}^2 \backslash K, \\ u(x,k) = -u^{\text{inc}}(x,k), \quad x \in \partial K, \\ \lim_{|x|\to\infty} |x|^{1/2} \left[\left(\frac{x}{|x|}, \nabla_x u(x,k) \right) - iku(x,k) \right] = 0 \end{cases} \tag{1}$$

where the limit holds uniformly in all directions $\frac{x}{|x|}$.

In integral equation methods, the *direct approach* in constructing the solution of problem (1) is based on the single-layer representation

$$u(x,k) = -\int_{\partial K} \Phi_k(x,y)\eta(y,k)ds(y), \quad x \in \mathbb{R}^2 \backslash K$$

where $\Phi_k(x, y) = \frac{i}{4} H_0^{(1)}(k|x - y|)$ is the fundamental solution of Helmholtz equation, and $H_0^{(1)}$ is the Hankel function of the first kind and order zero. This converts the scattering problem (1) into the determination of the unknown *normal derivative of the total field*

$$\eta(x, k) = \partial_{\nu(x)}(u(x, k) + u^{inc}(x, k)) \quad \text{on } \partial K.$$

The new unknown can then be recovered through uniquely solvable linear integral equations which can be expressed as linear operator equations of the second kind

$$(\mathcal{I} - \mathcal{R})\eta = f \tag{2}$$

in $L^2(\partial K)$. In this connection, the classical combined field integral equation (CFIE) [18] and the star combined integral equation (SCIE) [40] have been well understood in regards to their continuity and coercivity properties associated with the convex scattering problems. To allow the comparison of numerical results with the previous work on sound-soft scattering problems, we use here the CFIE for which equation (2) takes on the form

$$(I + \mathcal{K}' - ik\mathcal{V})\eta = 2(\partial_\nu - ik)u^{inc} \tag{3}$$

so that $\mathcal{R} = -\mathcal{K}' + ik\mathcal{V}$ and $f = 2(\partial_\nu - ik)u^{inc}$. In (3), I is the identity operator, ν is the exterior unit normal vector to ∂K, and $\mathcal{V}, \mathcal{K}'$ are the integral operators defined as

$$(\mathcal{V}\eta)(x) = 2\int_{\partial K} \Phi(x, y)\eta(y)ds(y), \quad x \in \partial K,$$
$$(\mathcal{K}'\eta)(x) = 2\int_{\partial K} \partial_{\nu(x)}\Phi(x, y)\eta(y)ds(y), \quad x \in \partial K.$$

Representation (2) is particularly useful in modeling the scattering phenomenon as a multiple-scattering problem when the scatterer K consists of disjoint obstacles. To elaborate on this, we assume that K is comprised of the disjoint obstacles $K_1, \ldots, K_N$ ($N \geq 2$). In this case, (2) can be rewritten as

$$\left(\begin{bmatrix} \mathcal{I}_1 & 0 & \cdots & 0 \\ 0 & \mathcal{I}_2 & \cdots & 0 \\ \vdots & \vdots & \ddots & \vdots \\ 0 & 0 & \cdots & \mathcal{I}_N \end{bmatrix} - \begin{bmatrix} \mathcal{R}_{11} & \mathcal{R}_{12} & \cdots & \mathcal{R}_{1N} \\ \mathcal{R}_{21} & \mathcal{R}_{22} & \cdots & \mathcal{R}_{2N} \\ \vdots & \vdots & \ddots & \vdots \\ \mathcal{R}_{N1} & \mathcal{R}_{N2} & \cdots & \mathcal{R}_{NN} \end{bmatrix}\right) \begin{bmatrix} \eta_1 \\ \eta_2 \\ \vdots \\ \eta_N \end{bmatrix} = \begin{bmatrix} f_1 \\ f_2 \\ \vdots \\ f_N \end{bmatrix} \tag{4}$$

where $\mathcal{I}_i$ is the identity operator on $L^2(\partial K_i)$, $\mathcal{R}_{ij}$ is the associated linear operator mapping $L^2(\partial K_j)$ into $L^2(\partial K_i)$, η_i and f_i are the restrictions of η and f onto ∂K_i. In order to conclude that η is the superposition of multiple-scattering effects, we first multiply equation (4) with the inverse of the diagonal operator

$$\mathcal{D} = \begin{bmatrix} \mathcal{I}_1 - \mathcal{R}_{11} & 0 & \cdots & 0 \\ 0 & \mathcal{I}_2 - \mathcal{R}_{22} & \cdots & 0 \\ \vdots & \vdots & \ddots & \vdots \\ 0 & 0 & \cdots & \mathcal{I}_N - \mathcal{R}_{NN} \end{bmatrix} \tag{5}$$

and obtain the equivalent operator equation

$$(\mathcal{I} - \mathcal{T})\eta = \mathfrak{f} \tag{6}$$

in $L^2(K)$ where

$$\mathcal{I} = \begin{bmatrix} \mathcal{I}_1 & 0 & \cdots & 0 \\ 0 & \mathcal{I}_2 & \cdots & 0 \\ \vdots & \vdots & \ddots & \vdots \\ 0 & 0 & \cdots & \mathcal{I}_N \end{bmatrix}, \quad \mathcal{T} = \begin{bmatrix} 0 & \mathcal{T}_{12} & \cdots & \mathcal{T}_{1N} \\ \mathcal{T}_{21} & 0 & \cdots & \mathcal{T}_{2N} \\ \vdots & \vdots & \ddots & \vdots \\ \mathcal{T}_{N1} & \mathcal{T}_{N2} & \cdots & 0 \end{bmatrix} \quad \text{and} \quad \mathfrak{f} = \begin{bmatrix} \mathfrak{f}_1 \\ \mathfrak{f}_2 \\ \vdots \\ \mathfrak{f}_N \end{bmatrix} \tag{7}$$

with

$$\mathcal{T}_{ij} = (\mathcal{I}_i - \mathcal{R}_{ii})^{-1}\mathcal{R}_{ij} \qquad \text{and} \qquad \mathfrak{f}_i = (\mathcal{I}_i - \mathcal{R}_{ii})^{-1} f_i.$$

Next, we observe that, when the spectral radius of $\mathcal{T}$ is less than 1, the solution of (6) is given by the Neumann series

$$\eta = \sum_{m=0}^{\infty} \eta^m \qquad \text{with} \quad \eta^m = \mathcal{T}^m \mathfrak{f} \tag{8}$$

which represents η as the superposition of *multiple-scattering effects* η^m.

Remark 1 It is not known exactly what geometrical conditions would imply that the spectral radius of the operator T is less that 1. However, in the context of two smooth strictly convex obstacles, a semi-rigorous proof is presented in [8, §6]; additionally, in the context of several smooth convex obstacles illuminated by a plane wave incidence and satisfying appropriate geometrical constraints, the convergence of Neumann series is discussed in the asymptotic sense ($k \gg 1$) for its rearrangement into "primitive periodic orbits" is discussed in [25] implying, in particular, its convergence for two smooth strictly convex obstacles.

Note further that, denoting the restriction of η^m onto ∂K_i by η_i^m ($i = 1, \ldots, N$), representation (8) implies that

$$\eta_i^0 = \mathfrak{f}_i \tag{9}$$

and

$$\eta_i^m = \sum_{\substack{1 \le j \le N \\ j \ne i}} \mathcal{T}_{ij}\eta_j^{m-1} \qquad (m > 0). \tag{10}$$

Therefore η_i^m is the surface current generated on ∂K_i by (a) the incident field u^{inc} ignoring the other $N-1$ obstacles for $m = 0$, and (b) the fields scattering off the other $N-1$ obstacles at the $(m-1)th$ iteration for $m > 0$. Accordingly, when $N = 2$, (9) and (10) dismantle the scattering problem (2) into a recursive solution of single-scattering problems. When $N > 2$, a further decomposition is necessary to achieve this. Indeed, setting $\eta_{ij}^m = \mathcal{T}_{ij}\eta_j^{m-1}$ ($j \ne i$) for $m > 0$, we clearly have

$$\eta_i^m = \sum_{\substack{1 \le j \le N \\ j \ne i}} \eta_{ij}^m,$$

and repeating this process inductively we deduce that

$$\eta_i^m = \sum \eta_{\sigma_m, \ldots, \sigma_0} \qquad (m > 0) \tag{11}$$

where

$$\eta_{\sigma_m, \ldots, \sigma_0} = \mathcal{T}_{\sigma_m\sigma_{m-1}} \cdots \mathcal{T}_{\sigma_1\sigma_0}\mathfrak{f}_{\sigma_0} \tag{12}$$

and the summation is over all sequences $\{\sigma_j\}_{j=0}^m \subset \{1,\dots,N\}$ such that $\sigma_m = i$ and $\sigma_j \neq \sigma_{j+1}$ for $j = 0,\dots,m-1$. Therefore, setting

$$\eta_{\sigma_0} = \mathfrak{f}_{\sigma_0} \text{ on } K_{\sigma_0} \quad \text{and} \quad \eta_{\sigma_j,\dots,\sigma_0} = \mathcal{T}_{\sigma_j\sigma_{j-1}}\eta_{\sigma_{j-1},\dots,\sigma_0} \text{ on } K_{\sigma_j}\ (j = 1,\dots,m),$$

we finally deduce that determination of $\eta_{\sigma_m,\dots,\sigma_0}$ demands the recursive solution of single-scattering integral equations

$$(\mathcal{I}_{\sigma_j} - \mathcal{R}_{\sigma_j\sigma_j})\eta_{\sigma_j,\dots,\sigma_0} = g_{\sigma_j,\dots,\sigma_0} \text{ on } K_{\sigma_j}, \qquad j = 0,\dots,m, \tag{13}$$

where

$$g_{\sigma_j,\dots,\sigma_0} = \begin{cases} f_{\sigma_0}, & j = 0, \\ \mathcal{R}_{\sigma_j\sigma_{j-1}}\eta_{\sigma_{j-1},\dots,\sigma_0}, & 1 \le j \le m. \end{cases} \tag{14}$$

Consequently, (8), (9), (11), and (13) provide a complete decomposition of the scattering problem (2) into single-scattering contributions.

The foregoing argument reveals that efficient computation of η_i^m ($m \ge 0$) requires efficient solution of the sequence of single-scattering integral equations in (13). In view of this, let us mention that the rigorous high-frequency Galerkin boundary element methods in [23,24] are specifically designed for the effective solution of single-scattering integral equation (2) in configurations wherein the scatterer K consists of a single obstacle (in which case the integral equations (2) and (13) clearly coincide when $j = 0$) that does not allow for multiple-scattering of waves (in the sense that a ray with direction α initially hitting the obstacle K does not return to K after a geometrical reflection). In detail, the Galerkin approximation spaces in [23,24] are constructed based on the observation that, in this case, η can be factored into the product of a highly-oscillatory exponential with the phase $\varphi(x) = \alpha \cdot x$ and a slowly varying amplitude as

$$\eta(x,k) = e^{ik\,\varphi(x)}\,\eta^{\text{slow}}(x,k), \qquad x \in \partial K. \tag{15}$$

This implies that, in order to eliminate the oscillations in η with increasing wavenumber k, the Galerkin approximation spaces $\hat{X}$ in $L^2(\partial K)$ must be constructed in the form

$$\hat{X} = e^{ik\,\varphi(x)}\,\hat{Y}. \tag{16}$$

Representations (15) and (16), in turn, imply that the approximation spaces $\hat{Y}$ must be designed to resemble the asymptotic behavior of the amplitude η^{slow} with increasing k in order to guarantee the efficient (frequency independent) solution of the integral equation (2). Indeed, as was shown in [23,24], the design of optimal approximation spaces can be based on a fine analysis on the wavenumber explicit derivative estimates of the amplitude η^{slow}.

The preceding discussion clarifies the approach that must be utilized in extending the algorithms in [23,24] for the (rigorous) iterative solution of integral equations in (13). More precisely, one has to identify the phases of the *multiple-scattering iterations* $\eta_{\sigma_j,\dots,\sigma_0}$, and derive wavenumber explicit estimates on the derivatives of the related amplitudes. Let us note in this connection that, when the obstacles $K_1,\dots,K_N$ are (i) *strictly convex*, and they satisfy (ii) the *no-occlusion condition* (in the sense that no line with the direction α passes through both K_i and K_j for $1 \le i \ne j \le N$; see Fig. 1a) along with (iii) the *visibility condition* (in the sense that the closed convex hull of any two obstacles intersects trivially with any one of the remaining obstacles; see Fig. 1b), the phases of $\eta_{\sigma_j,\dots,\sigma_0}$ are uniquely determined, and sharp wavenumber explicit estimates on the derivatives of the related amplitudes can be derived [25]. In the rest of the paper, we, therefore, assume that the obstacles $K_1,\dots,K_N$ satisfy these three purely geometrical conditions.

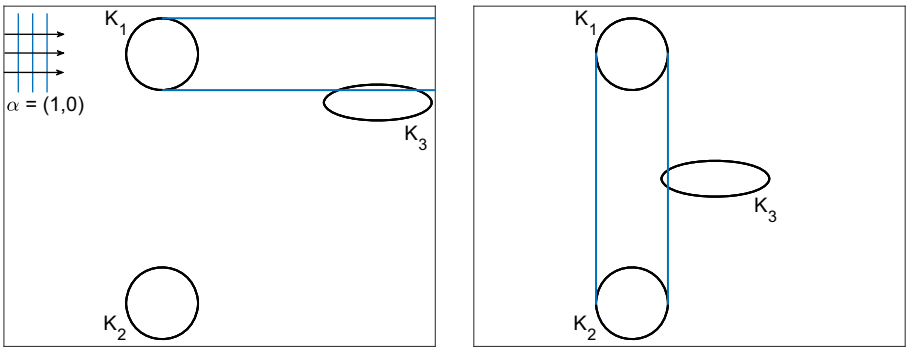

(a) Occlusion condition **(b)** Visibility condition

Fig. 1 Three obstacle configurations violating the **a** occlusion condition and **b** visibility condition

3 Phase Extraction and *k*-Explicit Derivative Estimates

As the line of reasoning in the preceding section shows, in order to delineate the details in extending the single-scattering algorithms in [23,24] to multiple-scattering problems, we first have to describe the phases of the multiple scattering iterations and discuss the wavenumber explicit estimates on the derivatives of the related amplitudes. To this end, it is sufficient to consider an arbitrary sequence $\{\sigma_m\}_{m=0}^{\infty} \subset \{1, \ldots, N\}$ such that $\sigma_{m+1} \neq \sigma_m$ for all m, and identify the phases φ_m of the solutions η_m of the integral equations

$$(\mathcal{I}_{\sigma_m} - \mathcal{R}_{\sigma_m,\sigma_m})\eta_m = g_m = \begin{cases} f_{\sigma_0}, & m = 0, \\ \mathcal{R}_{\sigma_m,\sigma_{m-1}}\eta_{m-1}, & m > 0. \end{cases} \tag{17}$$

In this case, each η_m can be factored into the product of a highly-oscillatory exponential modulated by a slowly varying amplitude as

$$\eta_m(x,k) = e^{ik\varphi_m(x)}\eta_m^{\text{slow}}(x,k), \qquad x \in \partial K_{\sigma_m}. \tag{18}$$

Indeed, as was shown in [25], the phase function φ_m is determined at any point $x \in \partial K_{\sigma_m}$ as

$$\varphi_m(x) = \begin{cases} \alpha \cdot x, & m = 0, \\ \alpha \cdot \mathcal{P}_0^m(x) + \sum_{j=0}^{m-1} |\mathcal{P}_{j+1}^m(x) - \mathcal{P}_j^m(x)|, & m > 0. \end{cases}$$

When $m > 0$, the points $(\mathcal{P}_0^m(x), \ldots, \mathcal{P}_m^m(x)) \in \partial K_{\sigma_0} \times \cdots \times \partial K_{\sigma_m}$, termed as the "broken $(m+1)$-rays terminating at $x \in \partial K_{\sigma_m}$," are uniquely determined by the geometrical conditions

$$\begin{cases} \text{(i) } \mathcal{P}_m^m(x) = x, \\ \text{(ii) } \alpha \cdot \nu(\mathcal{P}_0^m(x)) < 0, \\ \text{and, for } 0 \le j < m, \\ \text{(iii) } (\mathcal{P}_{j+1}^m(x) - \mathcal{P}_j^m(x)) \cdot \nu(\mathcal{P}_j^m(x)) > 0, \\ \text{(iv) } \dfrac{\mathcal{P}_1^m(x) - \mathcal{P}_0^m(x)}{|\mathcal{P}_1^m(x) - \mathcal{P}_0^m(x)|} = \alpha - 2\alpha \cdot \nu(\mathcal{P}_0^m(x))\,\nu(\mathcal{P}_0^m(x)), \\ \text{(v) } \dfrac{\mathcal{P}_{j+1}^m(x) - \mathcal{P}_j^m(x)}{|\mathcal{P}_{j+1}^m(x) - \mathcal{P}_j^m(x)|} = \dfrac{\mathcal{P}_j^m(x) - \mathcal{P}_{j-1}^m(x)}{|\mathcal{P}_j^m(x) - \mathcal{P}_{j-1}^m(x)|} \\ \qquad\qquad -2\dfrac{\mathcal{P}_j^m(x) - \mathcal{P}_{j-1}^m(x)}{|\mathcal{P}_j^m(x) - \mathcal{P}_{j-1}^m(x)|} \cdot \nu(\mathcal{P}_j^m(x))\,\nu(\mathcal{P}_j^m(x)). \end{cases} \tag{19}$$

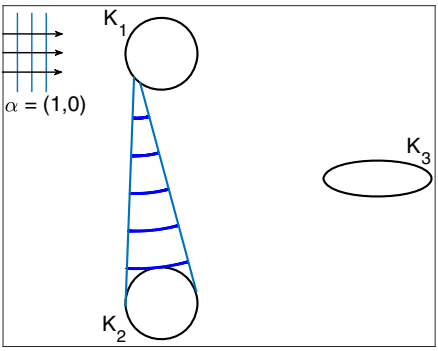

(a) Wavefronts: 1st reflections

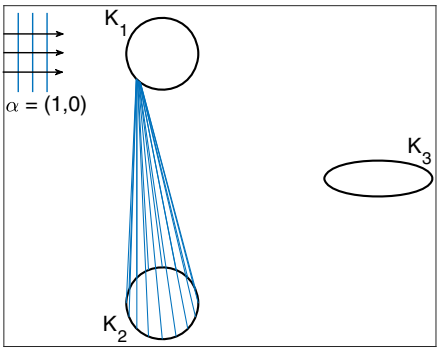

(b) Broken rays: 1st reflections

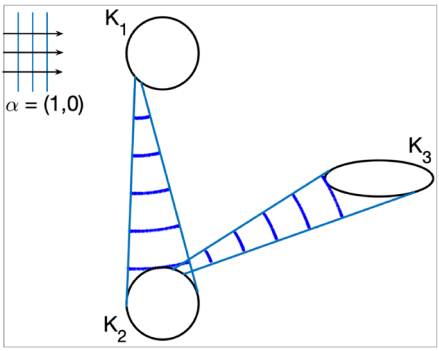

(c) Wavefronts: 2nd reflections

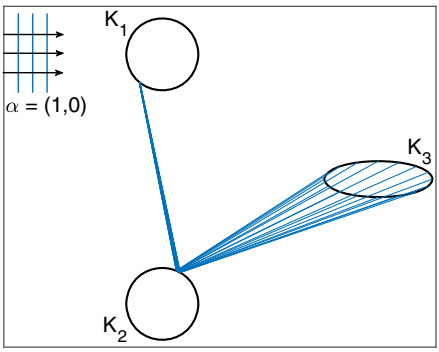

(d) Broken rays: 2nd reflections

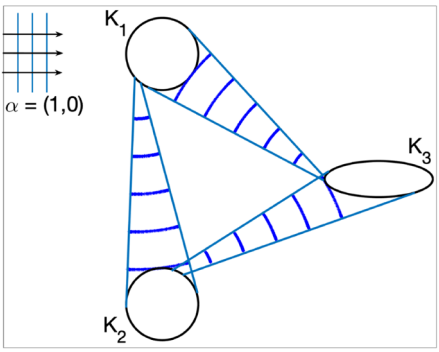

(e) Wavefronts: 3rd reflections

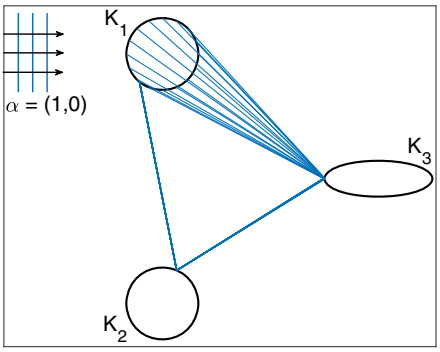

(f) Broken rays: 3rd reflections

Fig. 2 Left: Wavefronts generated by a planewave incidence with direction $\alpha = (0, 1)$ on the obstacle path K_1, K_2, K_3, K_1. Right: The associated broken rays in the first three reflections

Conditions (19) mean that, for any $x \in \partial K_{\sigma_m}$, the associated broken $(m + 1)$-ray $(\mathcal{P}_0^m(x), \ldots, \mathcal{P}_m^m(x))$ terminating at x is obtained by tracing the ray with initial direction α that arrives at x after precisely m geometrical reflections in the sense of the law of reflection. Indeed, wavefronts associated with the broken rays are convex at each reflection (see the left pane in Fig. 2) and this, in turn, implies that the ray paths become closer and closer with increasing number of reflections (see the right pane in Fig. 2); for a rigorous analysis of these facts we refer to [25].

Moreover, while the direction of incidence α identifies the *illuminated region*, *shadow boundaries*, and *shadow region* on ∂K_{σ_0} as

$$\begin{aligned}\partial K_{\sigma_0}^{IL} &= \left\{x \in \partial K_{\sigma_0} : \alpha \cdot \nu(x) < 0\right\}\\ \partial K_{\sigma_0}^{SB} &= \left\{x \in \partial K_{\sigma_0} : \alpha \cdot \nu(x) = 0\right\}\\ \partial K_{\sigma_0}^{SR} &= \left\{x \in \partial K_{\sigma_0} : \alpha \cdot \nu(x) > 0\right\},\end{aligned}$$

for $m > 0$ the broken rays determine the *illuminated regions*, *shadow boundaries*, and *shadow regions* on ∂K_{σ_m} as

$$\begin{aligned}\partial K_{\sigma_m}^{IL} &= \left\{x \in \partial K_{\sigma_m} : (\mathcal{P}_m^m(x) - \mathcal{P}_{m-1}^m(x)) \cdot \nu(x) < 0\right\}\\ \partial K_{\sigma_m}^{SB} &= \left\{x \in \partial K_{\sigma_m} : (\mathcal{P}_m^m(x) - \mathcal{P}_{m-1}^m(x)) \cdot \nu(x) = 0\right\}\\ \partial K_{\sigma_m}^{SR} &= \left\{x \in \partial K_{\sigma_m} : (\mathcal{P}_m^m(x) - \mathcal{P}_{m-1}^m(x)) \cdot \nu(x) > 0\right\}.\end{aligned}$$

As for the k-explicit estimates on the derivatives of the amplitude η_m^{slow}, we use L_m to denote the arc-length of ∂K_{σ_m}, and we choose $\gamma_m(s)$ to be a counterclockwise oriented L_m-periodic arc-length parameterization of ∂K_{σ_m} such that, for some $0 < t_m^{(1)} < t_m^{(2)} < L_m$,

$$\begin{aligned}\partial K_{\sigma_m}^{IL} &= \gamma_m((t_m^{(1)}, t_m^{(2)}))\\ \partial K_{\sigma_m}^{SB} &= \{\gamma_m(t_m^{(1)}), \gamma_m(t_m^{(2)})\}\\ \partial K_{\sigma_m}^{SR} &= \gamma_m((t_m^{(2)}, t_m^{(1)} + L_m)).\end{aligned}$$

Also, with a slight abuse of notation, we write $\eta_m^{\text{slow}}(s,k)$ for $\eta_m^{\text{slow}}(\gamma_m(s),k)$. The aforementioned estimates are now given in the following theorem where we use the standard convention that an empty sum is zero.

Theorem 1 *(k-explicit estimates on the derivatives of η_m^{slow}) For all $m, n \in \mathbb{N} \cup \{0\}$ and $k_0 > 0$, there exists a positive constant C independent of k and s such that*

$$\left|D_s^n \eta_m^{\text{slow}}(s,k)\right| \le C\left(k + \sum_{p=4}^{n+2}\left(k^{-1/3} + |w_m(s)|\right)^{-p}\right) \tag{20}$$

holds for all $k \ge k_0$ where $w_m(s) = (s - t_m^{(1)})(t_m^{(2)} - s)$.

Proof As was shown in [25, Theorem 3.2], estimate (20) holds for all sufficiently large k. That (20) holds for all $k \ge k_0$ is, therefore, a consequence of the fact that $D_s^n \eta_m^{\text{slow}}(s,k)$ depends continuously on s and k just as the parenthesized expression on the right-hand side of (20). □

Remark 2 Note that the proof of [25, Theorem 3.2] is based on [25, Theorem 3.1] which, in turn, is proved under the assumption that the conclusions of Theorem 2.1 and Corollary 2.1 there are valid for incident fields of the form

$$u(x) = e^{ik\psi(x)}\, u^{\text{slow}}(x), \qquad x \in O,$$

where O is an open set containing the smooth and strictly convex obstacle, ψ is a smooth phase function with smooth and convex wave-fronts $\{x : \psi(x) = t\}$ with respect to the normal

field $\nabla\psi$, and $u^{\text{slow}}(x) = u^{\text{slow}}(x, k)$ belongs to the Hörmander class $S^0_{1,0}(O \times (0, \infty))$ and has a classical asymptotic expansion

$$u^{\text{slow}}(x, k) \sim \sum_{p=0}^{\infty} k^{-p} A_p(x);$$

see Assumption C on page 289 in [25]. As was shown in [25], under the no-occlusion and visibility conditions, this assumption allows one to prove [25, Theorem 3.1] recursively.

4 Multiple-Scattering Galerkin Boundary Element Methods

In this section, we describe our approach in extending the Galerkin boundary element methods developed in [23,24] for the numerical solution of integral equations in (17) for any arbitrary sequence $\{\sigma_m\}_{m=0}^{\infty} \subset \{1, \ldots, N\}$ such that $\sigma_{m+1} \neq \sigma_m$ for all m. For simplicity of presentation, we write ∂K_m, ∂K_m^{IL}, ∂K_m^{SB} and ∂K_m^{SR} for ∂K_{σ_m}, $\partial K_{\sigma_m}^{\text{IL}}$, $\partial K_{\sigma_m}^{\text{SB}}$ and $\partial K_{\sigma_m}^{\text{SR}}$, and we let

$$\mathcal{S}_m = \mathcal{I}_{\sigma_m} - \mathcal{R}_{\sigma_m \sigma_m}. \tag{21}$$

In this case, equations (17) can be rephrased as the operator equations

$$\mathcal{S}_m \eta_m = g_m \tag{22}$$

in $L^2(\partial K_m)$, and the factorizations (18) motivate the first step in the construction of Galerkin approximation spaces for the solution of equations (22). Indeed, provided the operator $\mathcal{S}_m$ is bounded and strictly coercive, for any finite-dimensional subspace $\hat{X}_m$ of $L^2(\partial K_m)$, the Galerkin equation

$$\langle \hat{\mu}, \mathcal{S}_m \hat{\eta}_m \rangle = \langle \hat{\mu}, g_m \rangle, \quad \text{for all } \hat{\mu} \in \hat{X}_m \tag{23}$$

admits a unique solution $\hat{\eta}_m \in \hat{X}_m$, and Céa's lemma provides the error estimate

$$\|\eta_m - \hat{\eta}_m\| \leq \frac{C_m}{c_m} \inf_{\hat{\mu} \in \hat{X}_m} \|\eta_m - \hat{\mu}\| \tag{24}$$

where C_m and c_m are, respectively, the continuity and coercivity constants of $\mathcal{S}_m$. Accordingly, this inequality converts the problem of numerical solution of equations (22) into the design of Galerkin approximation spaces $\hat{X}_m$ in $L^2(\partial K_m)$ that best replicates the behavior of η_m. In this connection, the factorization (18) implies that, in order to eliminate the oscillations inherent in η_m, the spaces $\hat{X}_m$ must be constructed as

$$\hat{X}_m = e^{ik\varphi_m} \hat{Y}_m \tag{25}$$

for some appropriate finite-dimensional function spaces $\hat{Y}_m$ in $L^2(\partial K_m)$. Note that, in this case, inequality (24) takes on the form

$$\|\eta_m - \hat{\eta}_m\| \leq \frac{C_m}{c_m} \inf_{\hat{\mu} \in \hat{Y}_m} \|\eta_m^{\text{slow}} - \hat{\mu}\| \tag{26}$$

and this, in turn, implies that the spaces $\hat{Y}_m$ must be designed to mimic the asymptotic behavior of the amplitudes η_m^{slow} with increasing wavenumber k. As was shown in [23,24] for $m = 0$, optimal design of the spaces $\hat{Y}_0$ must be based on a detailed understanding of the wavenumber explicit estimates on the derivatives of η_0^{slow}. Let us note in this regard that Theorem 1 shows that these estimates have the same form for any $m \geq 0$. Therefore the algorithms, as well as

the associated convergence analyses, presented in [23,24] apply without any change to the solution of equations (22), except that the phase functions φ_m in (25) and the corresponding illuminated regions $\partial K_m^{\mathrm{IL}}$, shadow boundaries $\partial K_m^{\mathrm{SB}}$, and shadow regions $\partial K_m^{\mathrm{SR}}$ depend on m.

With these observations, we now describe the extensions of the Galerkin boundary element methods in [23,24] along with the corresponding convergence results for the iterative solution of multiple-scattering integral equations (21). To this end, we fix m and we identify $L^2(\partial K_m)$ with $L^2([0, L_m])$ through the L_m-periodic parameterization γ_m.

4.1 Frequency-Adapted Galerkin Methods for Multiple-Scattering Problems

Considering first the extension of *frequency-adapted Galerkin boundary element methods* developed in [24] for the solution of multiple-scattering problems (21), given $\ell \in \mathbb{N}$, we set

$$\epsilon_j = \frac{1}{3}\,\frac{2\ell - 2j + 1}{2\ell + 1}, \qquad j = 1 \ldots, \ell,$$

and define the *illuminated region*, *shadow region*, and the *shadow boundaries* as

$$\begin{aligned}
IL_m &= [t_m^{(1)} + \xi_1 k^{-1/3+\epsilon_1}, t_m^{(2)} - \xi_2 k^{-1/3+\epsilon_1}],\\
DS_m &= [t_m^{(2)} + \zeta_2 k^{-1/3+\epsilon_1}, L_m + t_m^{(1)} - \zeta_1 k^{-1/3+\epsilon_1}],\\
SB_m^1 &= [t_m^{(1)} - \zeta_1 k^{-1/3+\epsilon_\ell}, t_m^{(1)} + \xi_1 k^{-1/3+\epsilon_\ell}],\\
SB_m^2 &= [t_m^{(2)} - \xi_1 k^{-1/3+\epsilon_\ell}, t_m^{(2)} + \zeta_2 k^{-1/3+\epsilon_\ell}],
\end{aligned}$$

and the *illuminated transitions* and *shadow transitions* for $j = 1 \ldots, \ell$ as

$$\begin{aligned}
IT_{m,j}^1 &= [t_m^{(1)} + \xi_1 k^{-1/3+\epsilon_{j+1}}, t_m^{(1)} + \xi_1 k^{-1/3+\epsilon_j}],\\
IT_{m,j}^2 &= [t_m^{(2)} - \xi_2 k^{-1/3+\epsilon_j}, t_m^{(2)} - \xi_2 k^{-1/3+\epsilon_{j+1}}],\\
ST_{m,j}^1 &= [t_m^{(1)} - \zeta_1 k^{-1/3+\epsilon_j}, t_m^{(1)} - \zeta_1 k^{-1/3+\epsilon_{j+1}}],\\
ST_{m,j}^2 &= [t_m^{(2)} + \zeta_2 k^{-1/3+\epsilon_{j+1}}, t_m^{(2)} + \zeta_2 k^{-1/3+\epsilon_j}]
\end{aligned}$$

which are superfluous when $\ell = 1$. Here the positive constants $\xi_1, \xi_2, \zeta_1, \zeta_2$ are chosen so that these intervals are non-degenerate for $k > 1$, and

$$t_m^{(1)} - \xi_1 < t_m^{(2)} - \xi_2 \qquad \text{and} \qquad t_m^{(2)} + \zeta_2 < L_m + t_m^{(1)} - \zeta_1.$$

Using $[a_j, b_j]$ to denote these 4ℓ intervals, for a given $d \in \mathbb{N} \cup \{0\}$, we define the *frequency-adapted Galerkin approximation space* $\mathcal{A}_m^{\ell,d} \subset L^2([0, L_m])$ of dimension $4\ell(d+1)$ as

$$\mathcal{A}_m^{\ell,d} = \bigoplus_{j=1}^{4\ell} \chi_{[a_j,b_j]}\, e^{ik\,\varphi_m \circ \gamma_m}\, \mathbb{P}_d \tag{27}$$

where $\mathbb{P}_d$ is the vector space of univariate polynomials of degree at most d.

The approximation properties of the resulting Galerkin boundary element methods are given in the next theorem.

Theorem 2 *Suppose that $\mathcal{S}_m$ is continuous with a continuity constant C_k and coercive with a coercivity constant c_k for all $k > k_0$ for some $k_0 \geq 1$. Suppose further that $\ell \in \mathbb{N}$ and*

$d \in \mathbb{N} \cup \{0\}$ are given, and $\hat{\eta}_{m,\ell,d}$ is the unique solution of the Galerkin equation (23) for $\hat{X}_m = \mathcal{A}_m^{\ell,d}$. Then there exists a positive constant C independent of k such that

$$\frac{\|\eta_m - \hat{\eta}_{m,\ell,d}\|}{\|\eta_m\|} \leq C \frac{C_k}{c_k} \frac{\ell \left(1 + k^{\frac{n}{6\ell+3} - \frac{1}{2}}\right)}{d^n} \tag{28}$$

for all $n \in \{0, \ldots, d+1\}$ and all $k > k_0$.

Proof In light of Theorem 1, the proof follows the same lines as the proof of [24, Corollary 1]; see also [24, Remark 1]. □

Remark 3 As noted in [22, p.10] (see also the references therein), the stability constant C_k/c_k is in general unbounded as $k \to \infty$. We note in this connection the operator $\mathcal{S}_m$ is continuous for all $k > 0$ when it is related with the CFIE or SCIE, and it is coercive when $k \gg 1$ for CFIE and when $k > 0$ for SCIE, with $C_k/c_k = \mathcal{O}(k^{1/3})$ as $k \to \infty$ in both cases.

Remark 4 As detailed in [24, Remark 1], if ℓ increases proportionally with $\log k$ as k increases, then estimate (28) can be shown to imply

$$\frac{\|\eta_m - \hat{\eta}_{m,\ell,d}\|_{L^2(\partial K)}}{\|\eta_m\|_{L^2(\partial K)}} \leq C \frac{C_k}{c_k} \frac{\log k}{d^n}.$$

This, in turn, implies that the frequency-adapted Galerkin boundary element methods described above can be tailored so that *an increase of $\mathcal{O}(k^\varepsilon)$ in the number of degrees of freedom $4\ell\,(d+1)$ is sufficient to retain any given accuracy with increasing wavenumber k.*

Let us note that incorporating sufficiently many terms in the asymptotic expansion of η_m^{slow} into the problem formulation one can improve estimate (28). Indeed, as shown in [25], over the entire boundary ∂K_m, $\eta_m^{\text{slow}}(x,k)$ belongs to the Hörmander class $S^1_{2/3,1/3}(\partial K_m \times (0,\infty))$ and admits the asymptotic expansion

$$\eta_m^{\text{slow}}(x,k) \sim \sum_{p,q\geq 0} a_{m,p,q}(x,k) = \sum_{p,q\geq 0} k^{2/3-2p/3-q}\, b_{m,p,q}(x) \Psi^{(p)}(k^{1/3} Z_m(x)) \tag{29}$$

where $b_{m,p,q}(x)$ are complex-analytic functions, $Z_m(x)$ is a real-valued smooth function (positive on the illuminated region, negative on the shadow region, and vanishes precisely to first order on the shadow boundary), and the function Ψ admits the asymptotic expansion

$$\Psi(\tau) \sim \sum_{j=0}^{\infty} c_j \tau^{1-3j} \qquad \text{as } \tau \to \infty,$$

and it is rapidly decreasing in the sense of Schwartz as $\tau \to -\infty$. If $a_{m,p,q}$ is incorporated into the problem formulation for (p,q) satisfying $2p/3 + q < \beta(r)$ where $\beta(0) = 0$ and $\beta(r) = \frac{r+1}{3}$ $(r \in \mathbb{N})$, then (as in [22]) one obtains the estimate

$$\frac{\|\eta_m - \hat{\eta}_{m,\ell,d}\|_{L^2(\partial K)}}{\|\eta_m\|_{L^2(\partial K)}} \leq C \frac{C_k}{c_k} \frac{1}{k^{\beta(r)}} \frac{\ell \left(1 + k^{\frac{n}{6\ell+3} - \frac{1}{2}}\right)}{d^n} \tag{30}$$

which improves (28). Therefore, it follows that, for any given continuous and coercive integral equation formulation of the scattering problem, use of sufficiently many terms appearing in the asymptotic expansion of η_m^{slow} in the problem formulation guarantees the *frequency independent solvability of the scattering problem*; see Ecevit [22, Corollary 12]. In particular, for

the CFIE, knowledge of the leading term in the asymptotic expansion, namely $a_{m,0,0}$, would guarantee not only frequency independent solvability but in fact, the accuracy of numerical solutions would increase with increasing wavenumber k. However, explicit expressions for $a_{m,0,0}$ are not available for $m \geq 1$ around the shadow boundaries and the deep shadow regions (for $m = 0$, see Remark 13 in [22]), and this is left for future work.

4.2 Galerkin Methods Based on Frequency-Dependent Changes of Variables for Multiple-Scattering Problems

Considering next the extension of *Galerkin approximation spaces based on frequency-dependent changes of variables* presented in [23] for the solution of multiple-scattering problems (21), we choose positive constants $\xi_j, \xi_j', \zeta_j, \zeta_j'$ $(j = 1, 2)$ satisfying the conditions

$$t_m^{(1)} + \xi_1 \leq t_m^{(1)} + \xi_1' = t_m^{(2)} - \xi_2' \leq t_m^{(2)} - \xi_2$$

and

$$t_m^{(2)} + \zeta_2 \leq t_m^{(2)} + \zeta_2' = L_m + t_m^{(1)} - \zeta_1' \leq P + t_m^{(1)} - \zeta_1.$$

For $k > 1$, we define the *illuminated and shadow transition* intervals as

$$IT_m^1 = [t_m^{(1)} + \xi_1 k^{-1/3}, t_m^{(1)} + \xi_1'] \qquad ST_m^1 = [t_m^{(1)} - \zeta_1', t_m^{(1)} - \zeta_1 k^{-1/3}]$$
$$IT_m^2 = [t_m^{(2)} - \xi_2', t_m^{(2)} - \xi_2 k^{-1/3}] \qquad ST_m^2 = [t_m^{(2)} + \zeta_2 k^{-1/3}, t_m^{(2)} + \zeta_2']$$

and the *shadow boundary* intervals as

$$SB_m^1 = [t_m^{(1)} - \zeta_1 k^{-1/3}, t_m^{(1)} + \xi_1 k^{-1/3}] \quad SB_m^2 = [t_m^{(2)} - \xi_2 k^{-1/3}, t_m^{(2)} + \zeta_2 k^{-1/3}].$$

Using $[a_j, b_j]$ to denote these 6 intervals, given $d \in \mathbb{Z}_+$, we define the *Galerkin approximation space* $\mathcal{C}_m^d \subset L^2([0, L_m])$ *based on frequency-dependent changes of variables* of dimension $6(d + 1)$ as

$$\mathcal{C}_m^d = \bigoplus_{j=1}^{6} \chi_{[a_j, b_j]}\, e^{ik\,\varphi_m \circ \gamma_m}\, \hat{\mathbb{P}}_{m,j},$$

where

$$\hat{\mathbb{P}}_{m,j} = \begin{cases} \mathbb{P}_d \circ \phi_m^{-1}, & \text{if } [a_j, b_j] \text{ is a transition interval,} \\ \mathbb{P}_d, & \text{otherwise,} \end{cases}$$

and ϕ_m is the frequency-dependent change of variables defined on the transition intervals as

$$\phi_m(s) = \begin{cases} t_m^{(1)} + \left(\xi_1 + (\xi_1' - \xi_1)\,\dfrac{s - a_1}{b_1 - a_1}\right) \exp\left(-\dfrac{1}{3}\dfrac{b_1 - s}{b_1 - a_1} \log k\right), & s \in IT_m^1, \\ t_m^{(2)} - \left(\xi_2' + (\xi_2 - \xi_2')\,\dfrac{s - a_2}{b_2 - a_2}\right) \exp\left(-\dfrac{1}{3}\dfrac{s - a_2}{b_2 - a_2} \log k\right), & s \in IT_m^2, \\ t_m^{(1)} - \left(\zeta_1' + (\zeta_1 - \zeta_1')\,\dfrac{s - a_3}{b_3 - a_3}\right) \exp\left(-\dfrac{1}{3}\dfrac{s - a_3}{b_3 - a_3} \log k\right), & s \in ST_m^1, \\ t_m^{(2)} + \left(\zeta_2 + (\zeta_2' - \zeta_2)\,\dfrac{s - a_4}{b_4 - a_4}\right) \exp\left(-\dfrac{1}{3}\dfrac{b_4 - s}{b_4 - a_4} \log k\right), & s \in ST_m^2. \end{cases} \tag{31}$$

Convergence properties of the Galerkin approximation spaces $\mathcal{C}_m^d$ are given in the next theorem.

Theorem 3 *Suppose that $\mathcal{S}_m$ is continuous with a continuity constant C_k and coercive with a coercivity constant c_k for all $k > k_0$ for some $k_0 \geq 1$. Suppose also that $d \in \mathbb{N} \cup \{0\}$ is given, and $\hat{\eta}_{m,d}$ is the unique solution of the Galerkin equation (23) for $\hat{X}_m = \mathcal{C}_m^d$. Then there exists a positive constant C independent of k such that*

$$\frac{\|\eta_m - \hat{\eta}_{m,d}\|}{\|\eta_m\|} \leq C \frac{C_k}{c_k} \frac{(\log k)^{n+1/2}}{d^n} \tag{32}$$

for all $n \in \{0, \ldots, d+1\}$ and all $k > k_0$.

Proof Using Theorem 1, the proof follows as in the proof of [23, Corollary 3.1]. □

Remark 5 Similar comments as in Remark 4 apply to the Galerkin boundary element methods based on frequency-dependent changes of variables for multiple scattering problems. For details, we refer to Ecevit [22].

5 Numerical Results

Here we present examples to confirm the developments in this paper. As demonstrated in [24], *frequency-adapted Galerkin boundary element methods* exhibit better numerical accuracy when implemented with the choice $\ell = 2$ in (27) which corresponds to the use of 8 subregions over the boundary of each scatterer. Moreover, in this case, all our numerical tests have shown that the accuracy thereby obtained is almost the same as that produced by the *Galerkin boundary element methods based on frequency-dependent changes of variables* when the same number of degrees of freedom is utilized. Therefore here we present only numerical results based on *frequency-adapted Galerkin boundary element methods* for $\ell = 2$. For the implementation details relating to *frequency-adapted Galerkin boundary element methods* and *Galerkin boundary element methods based on frequency-dependent changes of variables*, we refer to Ecevit and Özen [24] and Ecevit and Eruslu [23].

In all the examples, we take the direction of incidence as $\alpha = (1, 0)$, and we display the number of reflections M versus the logarithmic relative error

$$\log_{10}\left(\frac{\|\eta - \mu_M\|_{L^2(\partial K)}}{\|\eta\|_{L^2(\partial K)}}\right) \tag{33}$$

associated to the local polynomial degrees $p = 4, 8, 12, 16, 20$ or $p = 4, 8, 12, 16$ for the wavenumbers $k = 50, 100, 200, 400$ and 800. In (33), η is a reference solution (taken as the *exact solution*) obtained through the numerical solution of a standard Nyström discretization [18] of the integral equation (3) using approximately 10 to 12 points per wavelength. On the other hand, μ_M is the numerical approximation of the Mth partial sum

$$\sum_{m=0}^{M-1} \eta^m \qquad (M \geq 1) \tag{34}$$

of the Neumann series (8) through use of the *frequency-adapted Galerkin boundary element methods*. More precisely, in (34) we approximate each η^m by the superposition of the numerical solution of the associated single-scattering integral equations (13) through utilization of the *frequency-adapted Galerkin boundary element methods*.

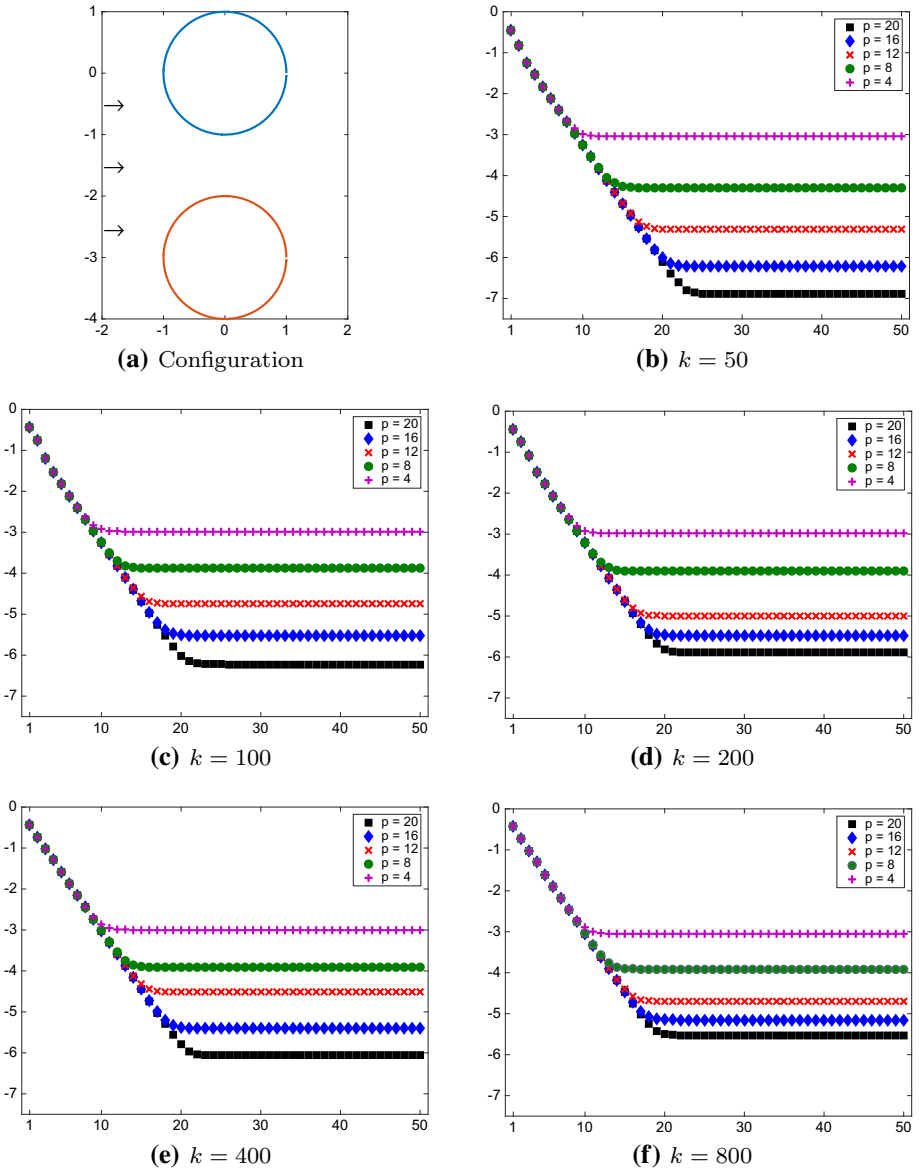

(a) Configuration **(b)** $k = 50$ **(c)** $k = 100$ **(d)** $k = 200$ **(e)** $k = 400$ **(f)** $k = 800$

Fig. 3 Number of reflections M versus logarithmic relative errors (33) for the polynomial degrees $p = 4, 8, 12, 16$

For concrete instances, we consider three different configurations consisting of either two three obstacles that are depicted in Figs. 3, 4 and 5.

Our first example concerns a multiple scattering configuration consisting of two unit circles centered at the points $(0, 0)$ and $(0, -3)$ where we consider reflections $M = 1, 2, \ldots, 50$. The results displayed in Fig. 3 show that, for any fixed value of k, the accuracy increases as the local polynomial degree p increases, for each fixed M. On the other hand, with increasing p the condition numbers of the stiffness matrices also increase in a manner roughly independent

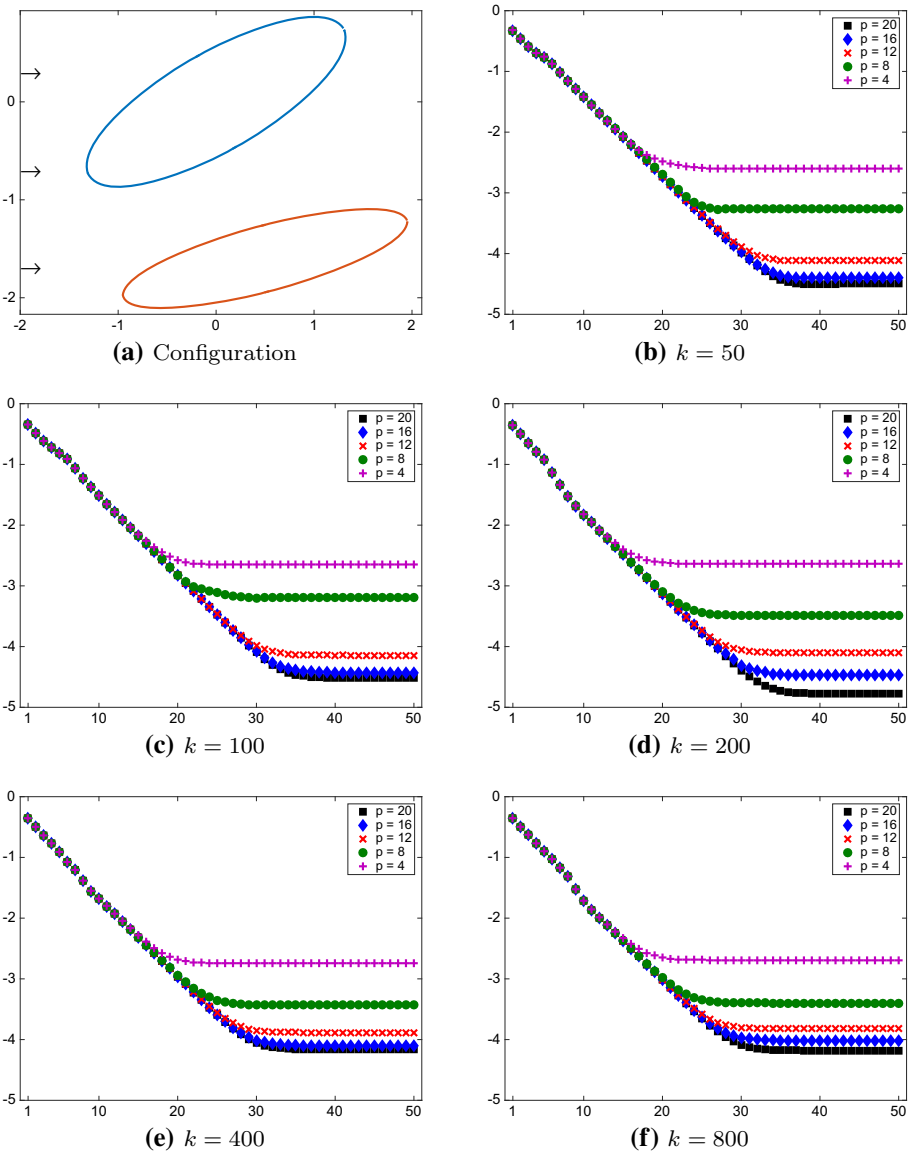

(a) Configuration **(b)** $k = 50$ **(c)** $k = 100$ **(d)** $k = 200$ **(e)** $k = 400$ **(f)** $k = 800$

Fig. 4 Number of reflections M versus logarithmic relative errors (33) for the polynomial degrees $p = 4, 8, 12, 16$

of the underlying wavenumber k (see the left pane in Fig. 6), and the accuracy stagnates even with increasing p; as evident from error plots in Fig. 3. We also note that for each k, the rate of decrease in errors with respect to the number of reflections is nearly identical until the accuracy provided by approximation space for the particular polynomial degree is reached, beyond which, obviously, there is no further improvement. Indeed, the slopes observed in these plots are consistent with the rate of convergence (as $k \to \infty$) of the Neumann series given in [25] as

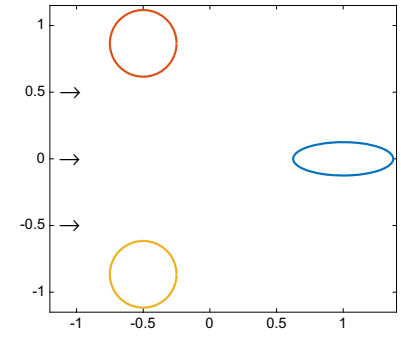

(a) Configuration

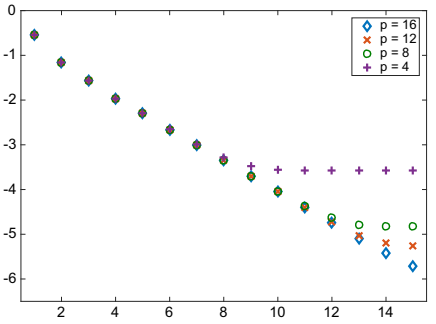

(b) $k = 50$

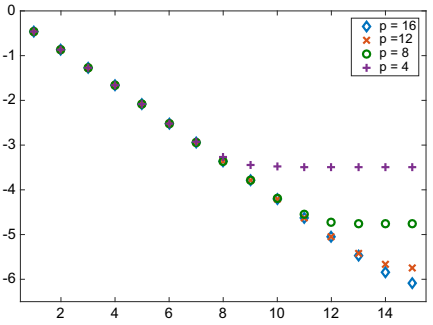

(c) $k = 100$

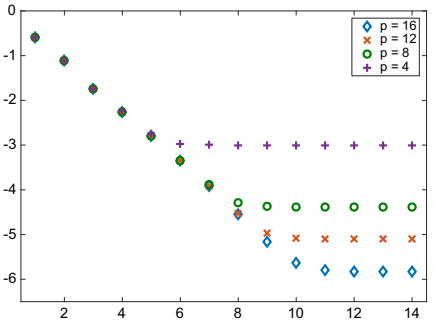

(d) $k = 200$

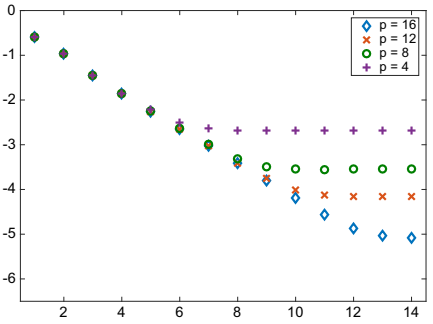

(e) $k = 400$

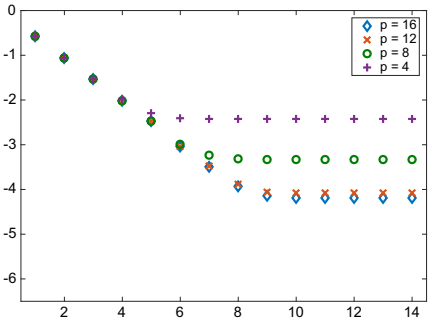

(f) $k = 800$

Fig. 5 Number of reflections M versus logarithmic relative errors (33) for the polynomial degrees $p = 4, 8, 12, 16$

$$\frac{1}{\sqrt{(1+d\kappa_1)(1+d\kappa_2)\left(1+\sqrt{1-\dfrac{1}{(1+d\kappa_1)(1+d\kappa_2)}}\right)}}$$

where d is the distance between the obstacles, and κ_1, κ_2 are the curvatures at the distance minimizing points.

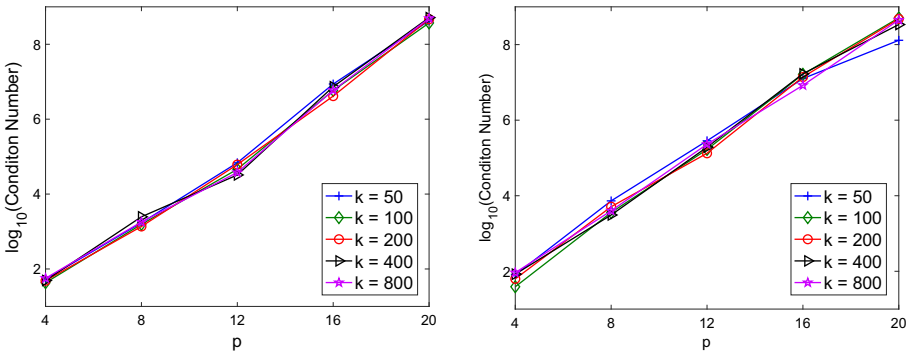

Fig. 6 Condition numbers of the Galerkin matrices versus the local polynomial degrees p at the 10th reflection on obstacle K_1 for the configurations in Fig. 3 (left) and Fig. 4 (right)

The second example presents a more challenging scattering geometry where the rate of convergence of the Neumann series is slower owing to the fact that the multiple-scattering rays are trapped longer in between the obstacles before they eventually leave. This particular configuration consists of two elliptical scatterers initially parameterized as $(\frac{3}{2}\cos t, \frac{1}{2}\sin t)$ and $(\frac{3}{2}\cos t, \frac{1}{3}\sin t)$ but having undergone counterclockwise rotations by $\pi/6$ and $\pi/12$ radians, respectively, where the latter is also translated by the vector $s = (0.5, -1.6)$. The results are presented in Fig. 4 for the reflections $M = 1, 2, \ldots, 50$. As we noted, in this case, the rate of convergence is slower requiring more reflections to reach a certain level of accuracy. Note further that there is only a marginal improvement in accuracy for the local polynomial degree $p = 20$ and, as we explained above, this again is related to the condition numbers of the associated stiffness matrices (see the right pane in Fig. 6).

The examples presented above concern configurations consisting only of two obstacles where the number of single-scattering integral equations (13) to be solved while computing the partial sum μ_M given in (34) is simply $2M$. On the contrary, this count grows exponentially with M when the number of obstacles N is more than 2. Indeed, in this case, it is straightforward to see that the computation of μ_M requires the solution of

$$N\,[1 + (N-1) + (N-1)^2 + \cdots + (N-1)^{M-1}] \tag{35}$$

number of single-scattering integral equations (13). This shows that the direct utilization of our algorithms is impractical when this number is large. This difficulty, however, can be overcome by employing a recently developed Krylov subspace method that retains the phase information associated with the multiple-scattering iterates and that thereby allows for the acceleration of convergence of the Neumann series [8]. This convergence can be further enhanced the through utilization of "dynamical Kirchhoff preconditioning" [8].

The nature of this kind of preconditioners, however, can "affect" the resulting conclusions concerning the accuracy of the final solution mainly because the illuminated regions change from one reflection to another. This represents a major difference when compared to classical preconditioners as explained in [8]. Therefore, for the sake of this paper, we will focus only on the accuracy provided by the algorithms developed herein. We therefore present, as a final example, a simple multiple-scattering example consisting of three obstacles. The configuration we consider is comprised of two circles of radius $\frac{1}{4}$ centered at $(-\frac{1}{2}, \pm\frac{\sqrt{3}}{2})$, and an ellipse parametrized as $(1 + \frac{3}{8}\cos t, \frac{1}{8}\sin t)$; see Fig. 5. In this particular implementation, we again observe similar behavior in the accuracy in terms of the rate of convergence and

increase in polynomial degree. Let us mention in the context of the speed of convergence that when the number of obstacles is more than two, the corresponding theoretical convergence rates (as $k \to \infty$) of the Neumann series are not known; rate of convergence formulas are available only on "periodic orbits" [4,25].

6 Conclusion

In this paper, we extended the single-scattering algorithms proposed in [23,24] to encompass the multiple-scattering problems in the exterior of finitely many smooth, compact, convex obstacles. In this connection, we showed that each single-scattering iterate can be approximated efficiently through the use of these algorithms. Indeed, as we showed, the Galerkin spaces proposed in this article have the capability of producing prescribed tolerances for arbitrary frequencies provided that the number of degrees of freedom is increased according to $\mathcal{O}(k^\epsilon)$ (for any $\epsilon > 0$) with increasing wavenumber k. Moreover, when sufficiently many terms in the asymptotic expansion of the multiple scattering iterations are incorporated into the problem formulation, these algorithms yield solutions for each single scattering iteration in a frequency independent operation count. Furthermore, the convergence of the Neumann series related to the multiple-scattering iterations can be significantly accelerated by a utilization of the Krylov subspace method along with the dynamical Kirchhoff preconditioning developed in [8]. Accordingly, these algorithms provide the first examples of rigorously error controllable procedures for the solution of multiple-scattering problems.

Compliance with ethical standards

Conflict of interest The authors declare that they have no conflict of interest.

References

1. Abboud, T., Nédélec, J.C., Zhou, B.: Méthode des équations intégrales pour les hautes fréquences. C. R. Acad. Sci. Paris Sér. I Math. **318**(2), 165–170 (1994)
2. Abboud, T., Nédélec, J.C., Zhou, B.: Improvements of the integral equation method for high frequency problems. In: Proceedings of 3rd International Conference on Mathematical Aspects of Wave Propagation Problems (1995)
3. Amini, S., Profit, A.: Multi-level fast multipole solution of the scattering problem. Eng. Anal. Bound. Elem. **27**(5), 547–564 (2003)
4. Anand, A., Boubendir, Y., Ecevit, F., Reitich, F.: Analysis of multiple scattering iterations for high-frequency scattering problems. II. The three-dimensional scalar case. Numer. Math. **114**(3), 373–427 (2010)
5. Antoine, X.: Advances in the on-surface radiation condition method: theory, numerics and applications. In: Magoulès, F. (ed.) Computational Methods for Acoustics Problems, pp. 169–194. Saxe-Coburg Publications, Stirlingshire (2008)
6. Banjai, L., Hackbusch, W.: Hierarchical matrix techniques for low- and high-frequency Helmholtz problems. IMA J. Numer. Anal. **28**(1), 46–79 (2008)
7. Boffi, D.: Finite element approximation of eigenvalue problems. Acta Numer. **19**, 1–120 (2010)
8. Boubendir, Y., Ecevit, F., Reitich, F.: Acceleration of an iterative method for the evaluation of high-frequency multiple scattering effects. SIAM J. Sci. Comput. **39**(6), B1130–B1155 (2017)
9. Bruno, O., Geuzaine, C., Reitich, F.: On the O(1) solution of multiple-scattering problems. IEEE Trans. Magn. **41**(5), 1488–1491 (2005)
10. Bruno, O.P., Domínguez, V., Sayas, F.J.: Convergence analysis of a high-order Nyström integral-equation method for surface scattering problems. Numer. Math. **124**(4), 603–645 (2013)

11. Bruno, O.P., Geuzaine, C.A.: An O(1) integration scheme for three-dimensional surface scattering problems. J. Comput. Appl. Math. **204**(2), 463–476 (2007)
12. Bruno, O.P., Geuzaine, C.A., Monro Jr., J.A., Reitich, F.: Prescribed error tolerances within fixed computational times for scattering problems of arbitrarily high frequency: the convex case. Philos. Trans. R. Soc. Lond. Ser. A Math. Phys. Eng. Sci. **362**(1816), 629–645 (2004)
13. Bruno, O.P., Kunyansky, L.A.: A fast, high-order algorithm for the solution of surface scattering problems: basic implementation, tests, and applications. J. Comput. Phys. **169**(1), 80–110 (2001)
14. Chandler-Wilde, S.N., Graham, I.G., Langdon, S., Spence, E.A.: Numerical-asymptotic boundary integral methods in high-frequency acoustic scattering. Acta Numer. **21**, 89–305 (2012)
15. Chandler-Wilde, S.N., Hewett, D.P., Langdon, S., Twigger, A.: A high frequency boundary element method for scattering by a class of nonconvex obstacles. Numer. Math. **129**(4), 647–689 (2015)
16. Chandler-Wilde, S.N., Langdon, S.: A Galerkin boundary element method for high frequency scattering by convex polygons. SIAM J. Numer. Anal. **45**(2), 610–640 (2007). (electronic)
17. Chandler-Wilde, S.N., Langdon, S., Mokgolele, M.: A high frequency boundary element method for scattering by convex polygons with impedance boundary conditions. Commun. Comput. Phys. **11**(2), 573–593 (2012)
18. Colton, D., Kress, R.: Inverse Acoustic and Electromagnetic Scattering Theory, Applied Mathematical Sciences, vol. 93. Springer, Berlin (1992)
19. Davies, R.W., Morgan, K., Hassan, O.: A high order hybrid finite element method applied to the solution of electromagnetic wave scattering problems in the time domain. Comput. Mech. **44**(3), 321–331 (2009)
20. Domínguez, V.: Filon–Clenshaw–Curtis rules for a class of highly-oscillatory integrals with logarithmic singularities. J. Comput. Appl. Math. **261**, 299–319 (2014)
21. Domínguez, V., Graham, I.G., Smyshlyaev, V.P.: A hybrid numerical-asymptotic boundary integral method for high-frequency acoustic scattering. Numer. Math. **106**(3), 471–510 (2007)
22. Ecevit, F.: Frequency independent solvability of surface scattering problems. Turk. J. Math. **42**(2), 407–422 (2018)
23. Ecevit, F., Eruslu, H.H.: A Galerkin BEM for high-frequency scattering problems based on frequency-dependent changes of variables. IMA J. Numer. Anal. **39**(2), 893–923 (2019)
24. Ecevit, F., Özen, H.Ç.: Frequency-adapted galerkin boundary element methods for convex scattering problems. Numer. Math. **135**(1), 27–71 (2017)
25. Ecevit, F., Reitich, F.: Analysis of multiple scattering iterations for high-frequency scattering problems. I. The two-dimensional case. Numer. Math. **114**(2), 271–354 (2009)
26. Engquist, B., Majda, A.: Absorbing boundary conditions for the numerical simulation of waves. Math. Comput. **31**(139), 629–651 (1977)
27. Gibbs, A., Chandler-Wilde, S., Langdon, S., Moiola, A.: A high frequency boundary element method for scattering by a class of multiple obstacles (2019). arXiv:1903.04449
28. Giladi, E.: Asymptotically derived boundary elements for the Helmholtz equation in high frequencies. J. Comput. Appl. Math. **198**(1), 52–74 (2007)
29. Givoli, D.: High-order local non-reflecting boundary conditions: a review. Wave Motion **39**(4), 319–326 (2004). New computational methods for wave propagation
30. Grote, M.J., Kirsch, C.: Nonreflecting boundary condition for time-dependent multiple scattering. J. Comput. Phys. **221**(1), 41–62 (2007)
31. Grote, M.J., Sim, I.: Local nonreflecting boundary condition for time-dependent multiple scattering. J. Comput. Phys. **230**(8), 3135–3154 (2011)
32. Groth, S., Hewett, D., Langdon, S.: A hybrid numerical-asymptotic boundary element method for high frequency scattering by penetrable convex polygons. Wave Motion **78**, 32–53 (2018)
33. Groth, S.P., Hewett, D.P., Langdon, S.: Hybrid numerical-asymptotic approximation for high-frequency scattering by penetrable convex polygons. IMA J. Appl. Math. **80**(2), 324–353 (2013)
34. Hesthaven, J., Warburton, T.: High-order accurate methods for time-domain electromagnetics. CMES Comput. Model. Eng. Sci. **5**(5), 395–407 (2004)
35. Hewett, D.P.: Shadow boundary effects in hybrid numerical-asymptotic methods for high-frequency scattering. Eur. J. Appl. Math. **26**(5), 773–793 (2015)
36. Hewett, D.P., Langdon, S., Chandler-Wilde, S.N.: A frequency-independent boundary element method for scattering by two-dimensional screens and apertures. IMA J. Numer. Anal. **35**(4), 1698–1728 (2014)
37. Hewett, D.P., Langdon, S., Melenk, J.M.: A high frequency hp boundary element method for scattering by convex polygons. SIAM J. Numer. Anal. **51**(1), 629–653 (2013)
38. Huybrechs, D., Vandewalle, S.: A sparse discretization for integral equation formulations of high frequency scattering problems. SIAM J. Sci. Comput. **29**(6), 2305–2328 (2007)
39. Langdon, S., Mokgolele, M., Chandler-Wilde, S.: High frequency scattering by convex curvilinear polygons. J. Comput. Appl. Math. **234**(6), 2020–2026 (2010)

40. Spence, E.A., Chandler-Wilde, S.N., Graham, I.G., Smyshlyaev, V.P.: A new frequency-uniform coercive boundary integral equation for acoustic scattering. Commun. Pure Appl. Math. **64**(10), 1384–1415 (2011)
41. Tong, M.S., Chew, W.C.: Multilevel fast multipole acceleration in the Nyström discretization of surface electromagnetic integral equations for composite objects. IEEE Trans. Antennas Propag. **58**(10), 3411–3416 (2010)